On the importance of heat and mass transfer coupling for the characterization of hygroscopic insulation materials

Patrick Perre, Arnaud Challansonnex, Julien Colin

Version of Record: https://www.sciencedirect.com/science/article/pii/S0017931018338511
Manuscript_70a469d9925e9c57840cd78ffd83e2c7

On the importance of heat and mass transfer coupling for the characterization of hygroscopic insulation materials

Patrick Perré [a,b,*], Arnaud Challansonnex[a], Julien Colin[a,b]

[a] *LGPM, CentraleSupélec, Université Paris-Saclay, 8-10 rue Joliot-Curie, 91 190 Gif-sur-Yvette, France*
[b] *LGPM, CentraleSupélec, Centre Européen de Biotechnologie et de Bioéconomie (CEBB), 3 rue des Rouges Terres, 51 110 Pomacle, France*

Abstract

This work is focused on mass transfer characterization of hygroscopic materials used for insulation, such as low density fiberboards (LDF). Due to their particular morphology, these panels present a very high mass diffusivity due to the connected gaseous phase together with a very low thermal conductivity. This combination of properties exacerbates the coupling between heat and mass transfer in transient state. Based on experimental data obtained with an original set-up and relevant simulations performed using a comprehensive physical formulation, a throughout vision of this question is proposed in the present study. In particular, we emphasize on:

- The impressive change in core temperature in terms of magnitude and duration,
- The great impact of the internal temperature gradient, which slows down mass diffusion,
- The dramatic error on mass diffusivity value if the coupling is ignored,
- The possible determination of thermal conductivity during transient sorption tests.

A dimensionless number N_c was derived to quantify the intensity of this coupling. Finally, a practical example is proposed that confirms the importance of heat and mass transfer coupling in the case of LDF, and at the same time, proves that this effect can be controlled and corrected by using a relevant physical formulation.

Keywords: experiment, identification, modelling, RH at back face, transient state

1. Introduction

Establishing good thermal performances of constructions is getting more and more challenging and designers need to model physical phenomena with great accuracy(Crawley et al., 2001; Woloszyn and Rode, 2008; Delgado et al., 2010). Among them, the strong influence of coupled heat and mass transfer on energy consumption is well established. This is especially true for renewable materials, which generally have a high moisture buffering effect (Osanyintola et al., 2006; Zhang et al., 2017). Consequently, Building Energy Simulations (BES) models must account for coupled heat and mass transfer (Rafidiarison

*Corresponding author
Email address: patrick.perre@centralesupelec.fr (Patrick Perré)

et al., 2015; Hens, 2015), which gave rise to a strong demand for mass transfer characterization: mass diffusivity and sorption isotherms (Feng et al., 2015; Steeman et al., 2010). In addition, due to side effects such as molecular relaxation, dual-scale effects, sorption hysteresis (Almeida et al., 2010; Rémond et al., 2018), these materials must be characterized in transient state as these materials never undergo constant conditions in buildings (Yi et al., 2016; Allinson and Hall, 2010). However, the characterization of hygroscopic materials is not simple as, due to the latent heat of vaporization, no mass transfer can occur without heat transfer. Consequently, the temperature field is not uniform in the sample, which induces gradients of saturated water vapor, well known to affect mass diffusion. The present work is focused on a particular family of building materials: Low Density Fiberboards (LDF) or other hygroscopic insulation materials. These materials have a large and connected gaseous phase together with an hygroscopic solid phase. This builds up a porous medium with presents, regarding mass transfer, a conductive phase interacting with a storage phase. Such media are likely to present dual-scale phenomena (Hornung, 1997; Almeida et al., 2010; Perré, 2010). In addition, molecular relaxation was also reported in lignocellulosic products (Crank, 1953; Wadsö, 1994; Olek et al., 2016). All these memory effects have a significant impact on the energy balance in building and deserve attention.
Indeed, the importance of the coupling between heat and mass transfer in this kind of materials became evident when we started to analyze more subtle phenomena such as dual-scale modeling or molecular relaxation. A rigorous study of these effects required careful experiments to be conceived and performed. However, when analyzing a series of experimental data obtained in our laboratory to address these phenomena, we observed a strong, unexpected, influence of thermal conductivity on the identified parameters. Due to their particular morphology, these materials present a very high mass diffusivity, together with a very low thermal conductivity. As these materials are highly hygroscopic, this combination of properties exacerbates the coupling between heat and mass transfer in transient state. This observation forced us to further investigate this dramatic effect of heat and mass coupling for these materials. Coupled heat and mass transfer in lignocellulosic products must therefore be carefully addressed before the memory effects can be seriously investigated.
The in-depth experimental and theoretical analysis proposed in the present paper and the warning message to the scientific community were motivated by this fact. Configurations in the present work were intentionally chosen to reduce the two memory effects reported in lignocellulosic products : molecular relaxation remains low at RH values less than 60% and for thick LDF slabs, the time constant due to dual-scale effects becoming smaller than macroscopic time constant of diffusion.
The paper is structured as follows. Section 2 is devoted to the experimental part. It includes the description of samples and the experimental configuration. Original experimental data are presented that emphasizes the importance of temperature overshoot in the centre of the slab. Section 3 details the general framework and assumptions of coupled heat and mass transfer formulation. An in-house computational model able to solve this set of equations is then used in section 4 to simulate the experimental test. Using physical parameters from literature, the simulation perfectly confirms the temperature overshoot. The effect of heat flux on the dynamic of mass transfer is further investigated using the computational code as a tool. Section 5 develops an analytical method that proposes a dimensionless number able to simply quantify the importance of coupling, as a function of material properties and sorption conditions. Finally, section 5 proposes and validates a practical rule to accurately determine the dimensionless mass diffusivity using the back-face method of the sample (Perré et al., 2015) even though this back-face is not perfectly

insulated regarding heat transfer.

2. Experiment

2.1. Experimental set-up

The material used in the present work is LDF ($160\,kg.m^{-3}$ low-density fiberboard produced by Steico, Munich, Germany). The experiment consists in submitting a sample face to a sudden variation of relative humidity (RH) and to record the evolution of RH on the opposite face (Perré et al., 2015). The experiment was designed to obtain 1-D transfer without any heat and mass flux at the back face of the sample (Fig. 1). For that purpose, a temperature/RH sensor (Sensirion SHT25, HDI Electronics, Perois, France) was placed between two 20-mm thick plates of LDF. Side effects were avoided by choosing large dimensions ($30\,cm \times 30\,cm$), which is more than 7 times the diffusion thickness. Finally, to avoid lateral water vapor leakages, the two superimposed LDF plates were coated with an aluminium foil glued to the lateral faces by epoxy resin. Since the sensor is placed in the middle of the plates, one can consider that the flux only occur in 1-D in the vertical direction. This double sample is placed inside a climatic chamber (HPP110, Memmert, Schwabach, Germany) to control external conditions. Good ventilation inside the chamber ensures a symmetrical convective flux on each side of the double sample. Three temperature/RH sensors are placed inside the chamber to record the actual conditions applied to the sample.

2.2. Experimental results

Figure 2 presents a typical example of experimental data. This test was performed for a double layer of LDF panel ($\rho = 160\,kg.m^{-3}$, thickness $= 2 \times 20mm$) for a stepwise change of RH from 20% to 40% at 35^oC. Low RH values were intentionally chosen to reduce the effect of molecular relaxation on the dynamic of sorption equilibrium (Olek et al., 2011; Wadsö, 1994). The RH measured at the back-face of the sample needs about 10 hours to reach the new external RH. This information was already used to identify the dimensionless mass diffusivity of the panel in the method proposed in (Perré et al., 2015). The novelty of this work is to also measure the temperature at the back-face of the sample as can be seen on figure 3. This value is relevant thanks to the experimental configuration: as the back-face of the sample is the value in the centre of two large plates, the assumption of 1-D transfer is valid and no artefact of heat transfer is likely to perturb the temperature value. As a result, we can observe an impressive temperature peak due to condensation: this peak is large in magnitude (more than 4^oC above the ambiance) and in duration (more than 10 hours, the same duration as for mass transfer). Temperature peaks due to coupling were already observed in previous studies on bio-based materials (Colinart et al., 2016; Lelievre et al., 2014; Seng et al., 2017) but, to the best of our knowledge, not with such an important magnitude and duration. The results presented here are therefore original, certainly because purely 1-D transfer can only be obtained with great care with insulation materials. The next section uses simulations performed using the comprehensive formulation of coupled heat and mass transfer to analyse this impressive coupling and its effect on material characterization.

3. Macroscopic formulation

A comprehensive physical formulation was used in the present work. More detailed information regarding this set of equations can be found in published works (Perré et al.,

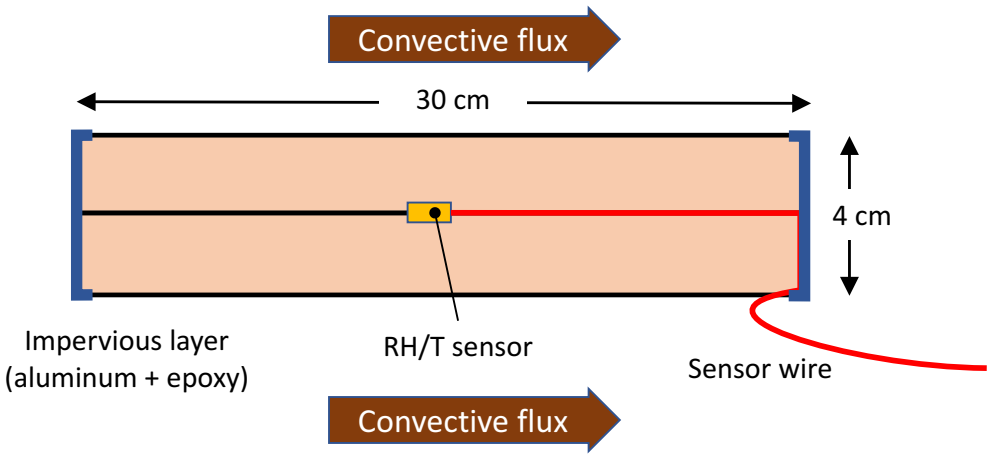

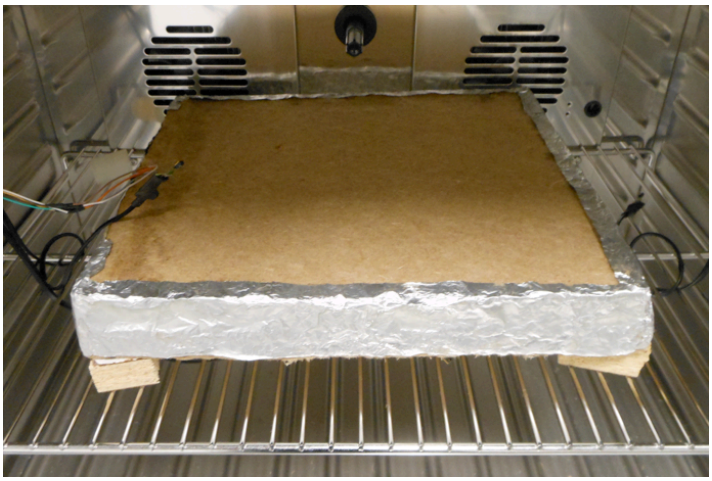

Figure 1: Schematic cross-sectional view of the double plate (top) and photograph of the sample placed inside the climatic chamber (bottom).

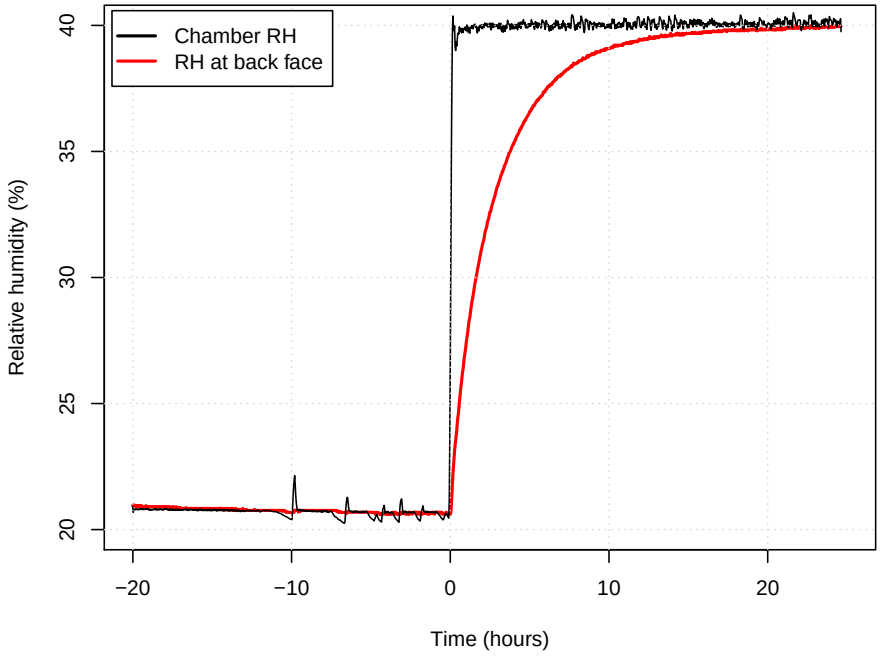

Figure 2: Experimental results for a double plate (2 x 20 mm) of LDF ($160\,kg.m^{-3}$): time evolution of relative humidity at back face on the plate.

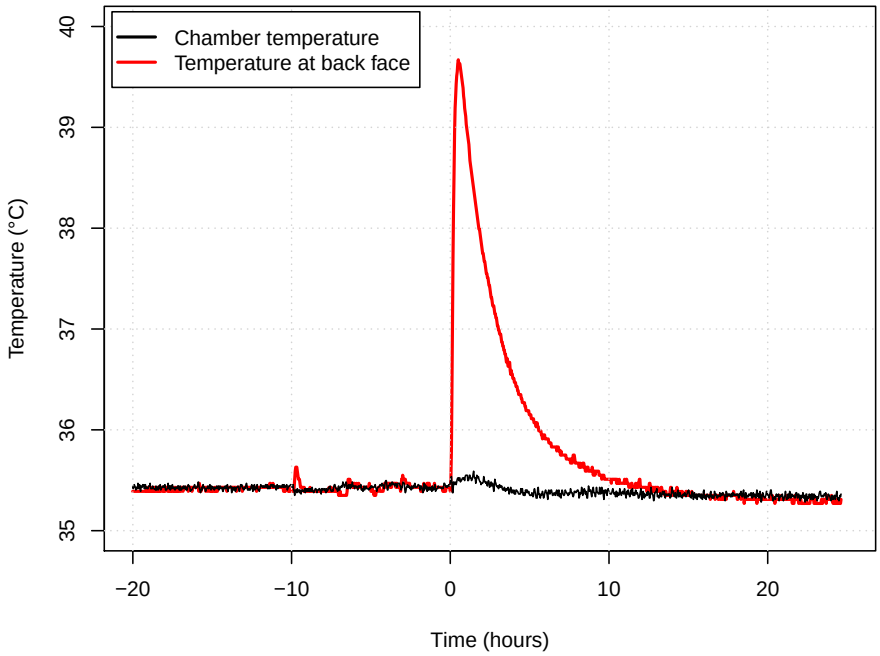

Figure 3: Experimental results for a double plate (2 x 20 mm) of LDF ($160\,kg.m^{-3}$): time evolution of temperature at back-face of the plate. The temperature peak ($39.7^{o}C$) occurs at 0.50 hour.

2007; Perré and Turner, 1999). In this model, suitable for bio-based materials, water exists in three different forms:

- liquid water inside the voids, that is transport by capillarity,
- bound water adsorbed by the fibers cell walls, that is transport by diffusion,
- water vapor inside the voids, that is transport by diffusion and gas advection,

For the sake of simplification, all liquid water contributions have been discarded, as the sample stays inside the hygroscopic domain. Similarly, considering the particular morphology of the material, one can make the hypothesis that a very large majority of the mass transfer occurs in the gaseous phase. Thus, the transport terms of bound water have been discarded. The simplified transport equations read as follows:

Moisture conservation

$$\rho_s \frac{\partial X}{\partial t} + \nabla \cdot (\rho_v \bar{\boldsymbol{v}}_g) = \nabla \cdot (\rho_g \boldsymbol{f} \boldsymbol{D}_v \cdot \nabla \omega_v) \tag{1}$$

Energy conservation

$$\begin{aligned} \frac{\partial}{\partial t}\left(\varepsilon_g(\rho_v h_v + \rho_a h_a) + \overline{\rho}_b \overline{h}_b + \varepsilon_s \rho_s h_s\right) + \nabla \cdot ((\rho_v h_v + \rho_a h_a)\bar{\boldsymbol{v}}_g) \\ = \nabla \cdot (\lambda_{eff} \nabla T + \rho_g \boldsymbol{f} \boldsymbol{D}_v (h_v \nabla \omega_v + h_a \nabla \omega_a)) \end{aligned} \tag{2}$$

Air conservation

$$\frac{\partial\left(\varepsilon_g \rho_a\right)}{\partial t} + \nabla \cdot (\rho_a \bar{\boldsymbol{v}}_g) = \nabla \cdot (\rho_g \boldsymbol{f} \boldsymbol{D}_v \nabla \omega_a) \tag{3}$$

Boundary conditions

$$\begin{aligned} &\boldsymbol{J}_w|_{x=0^+} \cdot \boldsymbol{n} = k\, c\, M_v\, \ln\left(\frac{1 - x_\infty}{1 - x_v|_{x=0}}\right) \\ &\boldsymbol{J}_q|_{x=0^+} \cdot \boldsymbol{n} = h\left(T|_{x=0} - T_\infty\right) \\ &P_g|_{x=0^+} = P_{atm} \end{aligned} \tag{4}$$

In the following equation, the barycentric mass velocities comes from the generalized Darcy's law

$$\bar{\boldsymbol{v}}_g = -\frac{\boldsymbol{K} \boldsymbol{k}_g}{\mu_g}(\nabla p_g - \rho_g \nabla \psi_{\boldsymbol{g}}) \tag{5}$$

The previous set of equations assumes that the porous medium is locally at equilibrium. This implies that :

- the temperature is the same for all phases $T_s = T_w = T_g$
- the partial pressure of water vapor inside the gaseous phase is related to the moisture content X *via* the sorption isotherm $p_v = p_{vs}(T) \times a(T, X)$, where function a is the sorption isotherm of the product, also called water activity, namely in food science.

The second assumption needs the phases to be locally at equilibrium. As stated in the introduction, hygroscopic insulation materials are likely to present two memory effects (dual-scale effect and molecular relaxation). Our team is currently working on a new formulation able to account for these effects at the macroscopic level (Perré, 2018). However, the present work is focused on the coupling between heat and mass and the configuration of interest limits the importance of the dual-scale effects, so that the classic macroscopic model might be used.

Further simplifications or assumptions allowed this set of equation to take this convenient form:

- the variation of partial densities inside the REV are negligible, so the intrinsic average is equal to the local value $\overline{\rho}_v^g = \rho_v$ and $\overline{\rho}_a^g = \rho_a$,
- the solid density is assumed to be constant $\rho_s = constant$,
- the moisture content X is used to consider the total amount of water present in the porous medium $\rho_s X = \varepsilon_g \overline{\rho}_v^g + \overline{\rho}_b$,
- the effective diffusivity is expressed as a function of the binary diffusivity of vapor in air : $\boldsymbol{D}_{eff} = \boldsymbol{f}\boldsymbol{D}_v$, where $\boldsymbol{f}$ is a dimensionless diffusivity tensor (indeed, along one given direction, $f = 1/\mu$ where μ is the *vapor resistance ratio* used for building materials),
- the pressure is supposed to be almost constant in terms of its absolute value. This means that the variation of pressure on the enthalpy balance can be omitted, while keeping the effect of its gradient in Darcy's law.

These equations are able to compute the coupling between heat and mass transfer occurring inside building materials. This set of equations allows three independent variables to be computed (for example, temperature or enthalpy, moisture content, air density or gaseous pressure). This is required, for example, if an important part of mass transfer occurs as convective flow (Darcy's regime).

4. Simulation results

The simulations are performed in 1-D for a 20-mm thick sample. The external conditions (T and RH) imposed at $x = 0\,mm$ correspond to the average of the three sensors placed inside the climatic chamber. At $x = 20\,mm$ (the back-face), the heat and mass fluxes are set to zero. Our reference test was simulated using the following physical parameters. The value of thermal conductivity ($\lambda_{eff} = 0.05\,W.m^{-1}.K^{-1}$) is determined by a classical mixture law using the gaseous and solid volume fractions and their conductivities (Louërat et al., 2018). The sorption isotherm is defined by the Hailwood-Horrobin model (Hailwood and Horrobin, 1946), using the adsorption envelop curve (Almeida et al., 2018): $RH/X = 2.76 + 15.84 \times RH - 15.26 \times RH^2$. The intrinsic permeability ($K = 6.5 \times 10^{-11} m^2$) comes from experimental measurements (Ai et al., 2017). With such a large permeability value, the barycentric movement of the gaseous phase induced by water vapor diffusion hardly alters the gaseous pressure, which remains very close to the atmospheric pressure. These physical phenomena are anyway considered in the model.
Finally, the dimensionless diffusivity is the sole parameter that was adjusted. Its value ($\boldsymbol{f} = 0.54$) was identified from the experimental RH evolution at the back-face as explained in (Perré et al., 2015). Both values are consistent with literature data (Vololonirina et al.,

2014; Rémond and Almeida, 2011). In particular, this value of $\boldsymbol{f}$ is in very good agreement with its determination from the real morphology of LDF using an upscaling method (Louërat et al., 2018).
Figure 4 depicts simulation results for the reference test. After the sudden increase in RH, water vapor condensates on the front face of the sample. By releasing the latent heat of vaporization, this moisture flux heats up the surface. Because of this temperature increase, the vapor pressure at the surface increases as well, as it is the product of water activity by the saturated vapor pressure, which increases rapidly with temperature. The primary effect of this change in surface vapor pressure is to reduce the external driving force, which slows down the process (Perré, 2015). This temperature increase eventually affects the whole sample, by a tricky coupling of heat and mass transfer: the temperature increase at one point increases the mass fraction of vapor, which gives rise to a vapor flux that condensates in neighboring parts. In turn, condensation increases the temperature further inside the medium, which allows the process to continue inwards. This produces a "heat wave" propagating towards the back-face, clearly visible on the temperature profiles. Once this wave reaches the back-face of the sample, a temperature gradient establishes towards the external face, to drive outwards the heat supplied in the medium via the latent heat of vaporization. In figure 4, the effect of this temperature gradient on the mass fraction of vapor is obvious, namely for the profiles at 10 and 30 minutes: although the internal value of moisture content (MC) is still close to the initial value, the mass fraction of vapor already increased significantly due to the temperature rise.

The model is also able to compute the time evolution of the two variables measured during the experiment: temperature and RH at the back face of the sample (Figures 5 and 6). The reference test is in perfect agreement with the experiment. For example, the temperature peak occurs at 0.47 hour for a maximum temperature equal to 39.8^oC. To further investigate the effect of heat and mass coupling, several virtual configurations were computed:

- **Modified thermal conductivity** ($\times 2$ and $\times 0.5$): these simulations exhibit the crucial effect of thermal conductivity, not only on the temperature overshoot (peak at respectively 38.6^oC and 41.2^oC instead of 39.8^oC). The peak time changes also significantly (peak respectively at 0.34h and 0.67h instead of 0.50h). Indeed, when the thermal conductivity decreases, heat dissipation is slowed down. Consequently the temperature peak is higher and shifted to larger times. The effect of the temperature field on the dynamic of RH evolution is also evident.

- **No heat and mass coupling:** the coupling is easily canceled by setting the latent heat of vaporization, Lv, to zero. Consistently, the temperature remains at the external temperature. As a consequence of the absence of coupling, the dynamic of RH evolution is much faster (2.5 hours instead of 4.3 hours for the reference test to attain 35% of RH). This confirms the importance of the heat and mass coupling on the global behavior,

- **No internal heat transfer**: setting the conductivity to zero cancels the heat flux inside the sample. Consequently, the latent heat of vaporization released by condensation cannot be driven towards the exchange face. A balance between water intake and temperature rise takes place: the amount of water condensed in the solid phase raises the temperature until the mass fraction of vapor equals the external value. The steady-state is obtained with an MC increase of 0.5% (against ca. 2% for the reference test) and a temperature of 43.4^oC. In this extreme, virtual, configuration, the coupling completely stops mass transfer !

Model	Value of $\boldsymbol{f}$ identified	Temperature peak
Reference test	0.54	39.8^oC
$\lambda = 0.5 \times \lambda_{ref}$	2.5	42.2^oC
$\lambda = 2 \times \lambda_{ref}$	0.38	38.1^oC
No coupling ($L_v = 0$)	0.28	35.0^oC

Table 1: Effect of modifying heat transfer on the identified value of $\boldsymbol{f}$ and on the peak temperature.

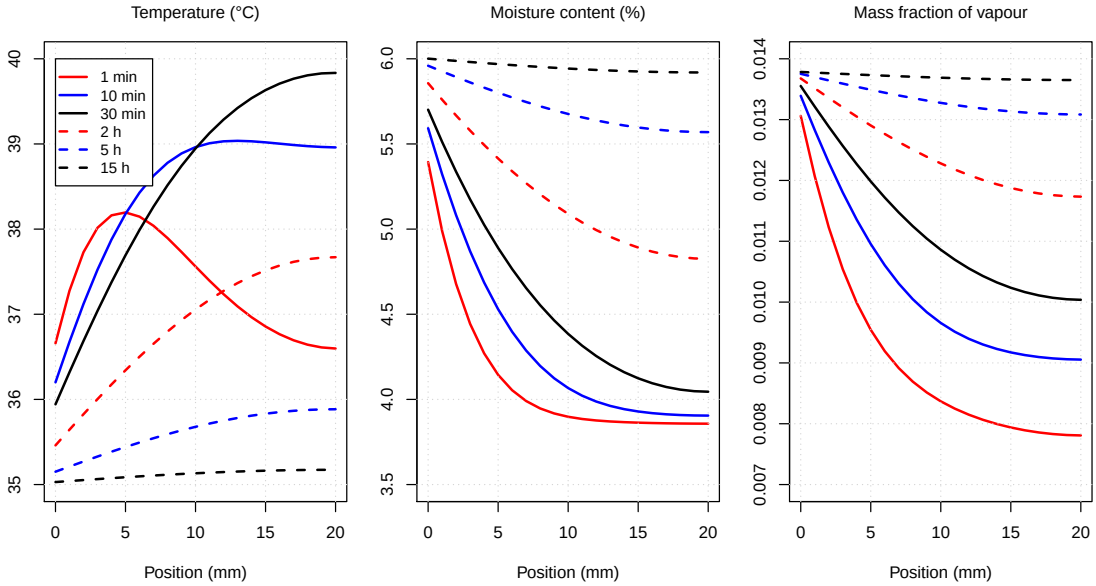

Figure 4: Profiles (the external face is at 0 mm and the symmetry plane at 20 mm) computed at selected times for the reference test ($\boldsymbol{f} = 0.54$ and $\lambda = 0.05\, W.m^{-1}.K^{-1}$).

In order to emphasize the effect of heat transfer on the identified value of $\boldsymbol{f}$, the experimental data was used as input data for the identification procedure with for several assumptions regarding heat conduction inside the sample . By inverse analysis, the $\boldsymbol{f}$ is then adjusted to get the best fit for RH evolution in spite of an wrong value for thermal conductivity (Table 1). In each case, the peak temperature was also recorded. For a lower thermal conductivity ($\times 0.5$), an unrealistic $\boldsymbol{f}$ value of 2.5 was obtained. Indeed, a diffusivity much larger than the diffusion of vapor in air is needed to compensate for the slowing of mass transfer due to the temperature gradient. In turns, this induces a large demand for latent heat of evaporation which produces a temperature peak at 42.2^oC. The effect is opposite when increasing the thermal conductivity ($\times 2$): $\boldsymbol{f}$ is reduced to 0.38 against 0.54 for the reference test and the temperature peak to 38.1^oC instead of 39.8^oC. The absence of heat and mass transfer coupling further reduces the value of $\boldsymbol{f}$ to 0.28. From these values, one has to notice that, when adapting the value of $\boldsymbol{f}$ to obtain the right kinetics for the RH evolution at back face, the effect on the temperature peak is even more important than for the simulation proposed in figures 6 and 5.
This set of identification suggests that the two pieces of information collected at the back face of the sample (RH and temperature) could possibly be used to identify two important parameters of insulation panels : dimensionless diffusivity $\boldsymbol{f}$ and thermal conductivity λ_{eff}.

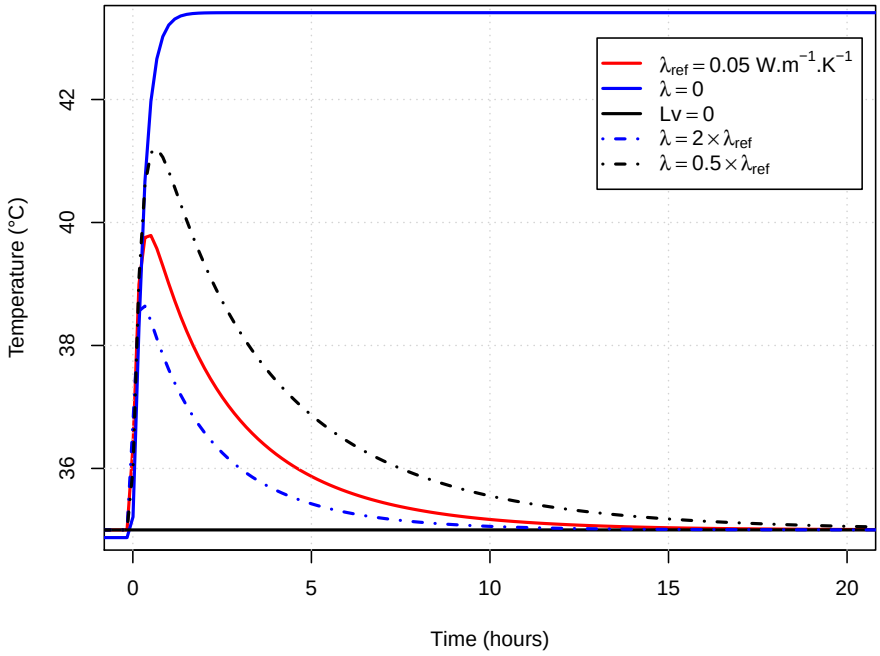

Figure 5: Simulation results for LDF ($160\,kg.m^{-3}$): evolution of temperature at the back-face of the plate during an adsorption step. The various virtual configurations tested are defined in the legend.

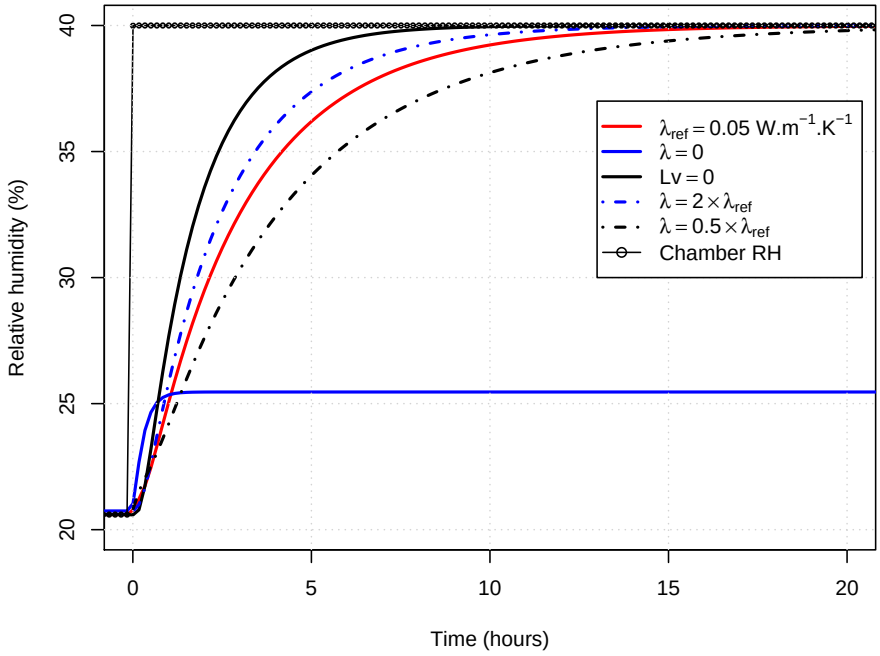

Figure 6: Simulation results for LDF ($160\,kg.m^{-3}$): evolution of relative humidity at the back-face of the plate during an adsorption step. The various virtual configurations tested are defined in the legend.

5. Analytical analysis

A simple analytical analysis is proposed in this section to express the temperature overshoot at the back-face of the sample. The local continuous expressions for the heat and vapor fluxes inside the medium (equations 1 and 2) are linearized over the sample thickness ℓ :

Vapour flux towards the sample core

$$q_v = -\rho_g \boldsymbol{f} \boldsymbol{D}_v \frac{\omega_{vL} - \omega_{v\infty}}{\ell} \tag{6}$$

Heat flux towards the exchange surface

$$q_h = -\lambda_{eff} \frac{T_L - T_\infty}{\ell} \tag{7}$$

Neglecting the heat required to heat-up the medium, the heat and mass fluxes are related via the latent heat of vaporization:

$$q_h = -L_v q_v \tag{8}$$

This assumption is quite classic as soon as evaporation or condensation is involved. For example, for a $200 kg.m^{-3}$ LDF board, an increase in moisture content of 4% represents an latent energy of $2.10^7\ J.m^{-3}$ while an increase in temperature of 5^oC requires $1.4.10^6\ J.m^{-3}$, only 7% of the latent energy.

In order to obtain a useful expression, further assumptions were made:

- A stepwise variation of RH is assumed, from RH_{ini} to RH_{fin}. The sample is supposed to be equilibrated at RH_{ini} at the beginning of the sudden change,
- As the peak is observed at short times, the heat and vapor flux will be expressed using this initial field,
- The effect of temperature on the vapor pressure is obtained by a first order development of the saturated vapor pressure curve,
- The gaseous density is supposed to be constant in time and in space.

With these assumptions, straightforward calculations allow equations (6-8) to be combined as follows :

$$\lambda_{eff} \Delta T = \boldsymbol{f} \boldsymbol{D}_v L_v \rho_{vs} \left(RH_{fin} - RH_{ini}(1 + \Delta T P'_{vs}/P_{vs}) \right) \tag{9}$$

$$\text{with} \quad \rho_{vs} = \frac{P_{vs} M_v}{RT}$$

The temperature increase, ΔT, can then be expressed as a proportion of $\Delta RH = RH_{fin} - RH_{ini}$:

$$\Delta T = \frac{\beta \Delta RH}{\lambda_{eff} + \beta\, RH_{ini}\, P'_{vs}/P_{vs}} \tag{10}$$

$$\text{with} \quad \beta = \boldsymbol{f} \boldsymbol{D}_v L_v \rho_{vs}$$

When expressing the saturated vapor pressure as an Arrhenius law ($P_{vs}(T) = P_0 exp(-E/RT)$), the ratio of derivative over the value becomes :

$$\frac{P'_{vs}}{P_{vs}} = \frac{E}{RT^2} \tag{11}$$

Applying expression (10) with the physical parameter values of LDF gives a temperature increase of 4.2^oC, which is close to that observed in our experiment or in our simulations. Note that this value does not depend on either the plate thickness nor the sorption isotherm (the amount of water gained by the sample during adsorption). This might be surprising but was confirmed by relevant simulations. Indeed, the thickness or the moisture buffering effect affects the global kinetics, not the value of temperature peak.

In equation (9), the impact of the heat and mass transfer coupling on the vapor flux q_v appears in the correction of RH at the sample core due to the temperature increase. When expressing this correction Δq_v as a proportion of the mass flux q_{v0}, one obtains the following ratio:

$$\frac{\Delta q_v}{q_v} = \frac{RH_{ini}\Delta T P_{vs}^{'}/P_{vs}}{\Delta RH - RH_{ini}\Delta T P_{vs}^{'}/P_{vs}} \tag{12}$$

Combining equation (12) with equations (10) leads to :

$$\frac{\Delta q_v}{q_v} = N_c \tag{13}$$

Where N_c, the coupling number, is a dimensionless number allowing the intensity of heat and mass transfer coupling to be quantified. Its reads as the product of three factors: i) the material properties, ii) the test configuration and iii) physical values :

$$N_c = \frac{\boldsymbol{f}}{\lambda_{eff}} \times \rho_{vs} RH_{ini} P_{vs}^{'}/P_{vs} \times \boldsymbol{D}_v L_v \tag{14}$$

In equation 14, the factor $RH_{ini}P_{vs}^{'}/P_{vs}$ accounts for the effect of temperature on vapor pressure. It involves the effect of sorption isotherm through the initial water activity value and the effect of temperature on the saturated vapor pressure. Therefore, for the same material, N_c depends on both the temperature level at which diffusion occur and the initial water activity of the product. In particular, N_c is proportional to RH_{ini}. For a test at 35^oC and an initial RH value of 20%, the order of magnitude of N_c is equal to 0.31 for LDF, 0.04 for MDF and 0.002 for wood in transverse direction. The first ratio involved in N_c confirms that the coupling is especially important for insulating materials having a large dimensionless value of vapor diffusivity. Note that the dimensionless factor is slightly underestimated as the computational simulations (Fig. 4) tells us that the temperature peak appears when the back face of the sample already gained some moisture : the factor RH_{ini} in equation (14) should then be somewhere between RH_{ini} and RH_{fin}.

6. Application

Recently, a new method was proposed to determine the mass diffusivity in unsteady-state by the inverse analysis of the RH evolution at the back face of the sample (Perré et al., 2015). In this method, the absence of mass transfer at the opposite face is ensured by a plate of hard PVC which holds a SHT25 temperature/RH sensor. In order to mimic this experiment, yet ensuring a proper 1-D configuration, the experimental device described in section 2.1 was used with a non-symmetrical configuration. One single 20-mm thick LDF plate was joined with a 15-mm thick plate of hard PVC, the temperature/RH sensor being placed at the interface between the two plates. In this case, the plane between the two plates is no longer a plane of symmetry: the absence of mass flux is ensured by the impervious PVC plate, but heat transfer can occur. The heat and mass coupling is therefore quite different from the symmetrical configuration presented in figures 2 and 3.

One part of the heat produced by condensation can now be evacuated through the PVC plate, reducing the temperature increase. In turn, this gradient of water vapor through the LDF plate is larger, which increases the mass flux. Compared to the symmetrical configuration, the experimental temperature peak is therefore dramatically reduced (Fig. 8) and the RH evolution significantly faster (Fig. 7).

On these figures, the simulations performed assuming a perfect symmetrical configuration with the $\boldsymbol{f}$ value previously identified (blue solid lines in figures 8 and 7), confirm the important effect of heat transfer at the back face of the sample. In order to consider this effect, an equivalent heat transfer coefficient was added to the simulation. This modified boundary condition assumes the PVC plate to be at steady state regarding heat transfer. This is reasonable as the characteristic time for thermal diffusion inside the PVC plate is smaller that the characteristic time of the coupled transfers in the LDF sample. This equivalent heat transfer coefficient coefficient $h_{back\,equivalent}$ was computed as two thermal resistances placed in series :

- the convective heat transfer coefficient between the PVC plate and the ambient, assumed to be equal to $15\,W.K^{-1}$
- the conduction in the 15-mm PVC plate ($\lambda_{PVC} \simeq 0.2\,W.m^{-1}.K^{-1}$ (DeCarvalho et al., 1996))

Thus, the value $h_{back\,equivalent} = 7.1\,W.K^{-1}$ was used for a new simulation (black solid lines in figures 8 and 7). The simulated results are now in very good agreement with the measurements. We can just notice a slight difference at short times just because the thermal inertia of the PVC plate is not considered in the modified boundary condition. The experimental temperature peak is therefore lower than the simulated value during the two first hours. This explains also the slightly higher experimental RH values at short times, due to the effect of temperature on the saturated vapor pressure. The good agreement found on both the RH and temperature evolution, without any fitted parameter, proves the relevance of the physical model and its prediction potential.

7. Conclusion

Based on experimental data obtained using an original set-up and relevant simulations performed using a comprehensive physical formulation, a throughout vision of the heat mass transfer in Low Density Fiberboards is proposed in the present study. In particular, we emphasize on:

- The impressive change in core temperature in terms of magnitude and duration,
- The great impact of the internal temperature gradient, which slows down mass diffusion,
- The dramatic error on mass diffusivity value if the coupling is ignored,
- The possibility to perfectly account for this coupling by using a relevant physical formulation.

A dimensionless numberN_c was derived to quantify the intensity of this coupling. Even though this number depends on the physical configuration, the most important factor is the ratio of mass over thermal diffusivity. The strong coupling between these phenomena

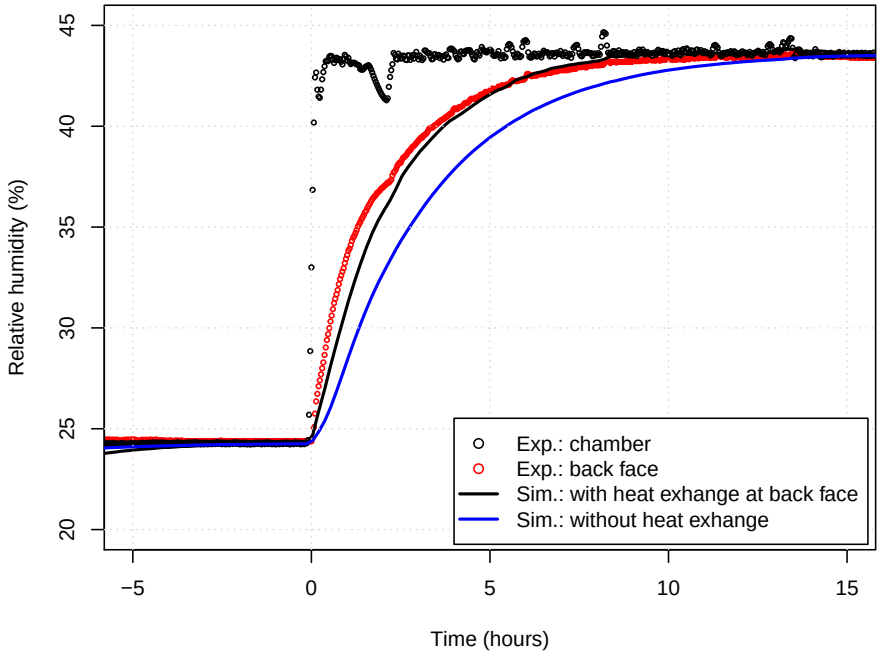

Figure 7: Experimental and simulated RH evolutions for a single plate (20 mm) of LDF ($160\,kg.m^{-3}$) placed over a plate of PVC.

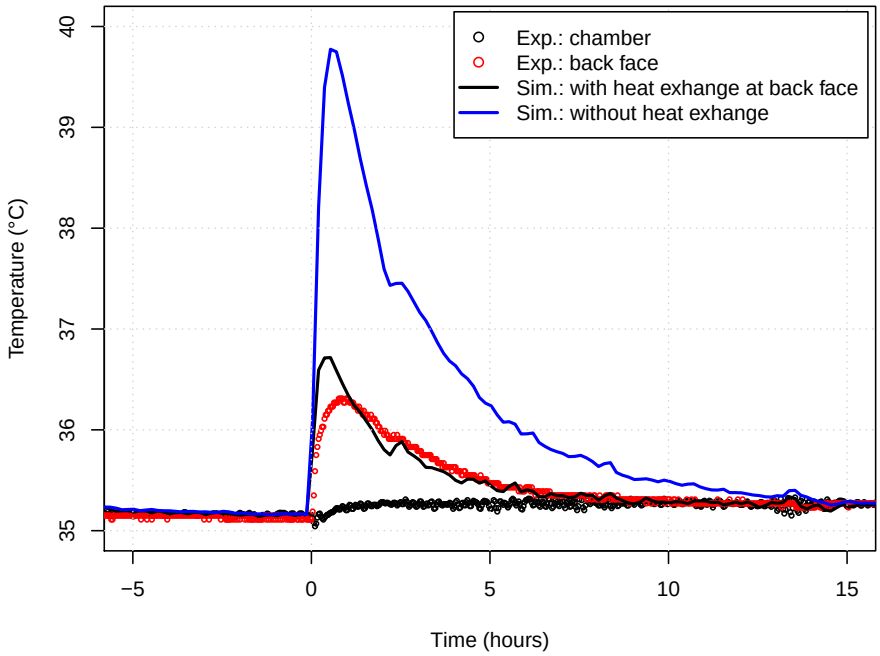

Figure 8: Experimental and simulated temperature evolutions for a single plate (20 mm) of LDF ($160\,kg.m^{-3}$) placed over a plate of PVC.

Table 2: List symbols (Latin letters)

Symbol	Name	Unit
a_w	sorption isotherm (water activity)	-
c	molar concentration	$mol.m^{-1}$
$\boldsymbol{D}$	diffusion tensor	$m^2.s^{-1}$
$\boldsymbol{f}$	dimensionless diffusion factor	-
h	specific enthalpy	$J.kg^{-1}$
h	heat transfer coefficient	$W.m^{-2}.K^{-1}$
E	activation energy of Arrhenius law	$J.mol^{-1}$
$\boldsymbol{J}_k$	diffusive flux of component k	$kg.m^{-2}.s^{-1}$
$\boldsymbol{J}_q$	heat flux	$W.m^{-2}$
K	intrinsic permeability	m^2
k	relative permeability	-
k	mass transfer coefficient	$m.s^{-1}$
L_v	specific enthalpy of evaporation	$J.kg^{-1}$
M	molar mass	$kg.mol^{-1}$
Nc	dimensionless coupling number	-
$\boldsymbol{n}$	normal unit vector	-
p or P	pressure	Pa
q_k	diffusive flux of component k	$kg.m^{-2}.s^{-1}$
q_h	heat flux	$W.m^{-2}$
R	gas constant	$J.mol^{-1}.K^{-1}$
T	temperature	$^{\circ}C$
$\boldsymbol{v}$	general velocity vector	$m.s^{-1}$
X	solid moisture content (dry basis)	-

forces us to be very careful when determining the unknown parameters by inverse analysis. To gain in robustness, several physical parameters must be measured during experiments in transient state. Besides, additional parameter values, such as thermal conductivity, could be determined by inverse method.

Notations

The main notation are summarized in tables (2 to 4)

References

Ai, W., Duval, H., Pierre, F., Perré, P., 2017. A novel device to measure gaseous permeability over a wide range of pressures: characterisation of slip flow for Norway spruce,

Table 3: List of symbols (Greek letters)

Symbol	Name	Unit
ε	volume fraction	-
λ	thermal conductivity	$W.m^{-1}.K^{-1}$
μ	vapor resistance ratio	-
ρ	density	$kg.m^{-3}$
∂	partial derivative	-
ψ	gravitational potential	s^{-2}
∇	gradient	-
$\nabla\cdot$	divergence	-
ω	mass fraction	-

Table 4: Subscripts and superscripts

Subscripts	Meaning
a	air
b	bound water
eff	effective property
g	relative to the gaseous phase
L	at the back face of the sample
s	solid
v	water vapor
vs	saturated water vapor
w	liquide water
∞	at large distance from interface

Superscript	Meaning
$\overline{\psi}$	averaged of variable ψ over the REV
$\overline{\psi}^{\ell}$	intrinsic average of ψ over phase ℓ

European beech, and wood-based materials. Holzforschung 71 (2), 147–162.
URL https://hal.archives-ouvertes.fr/hal-01523306

Allinson, D., Hall, M., 2010. Hygrothermal analysis of a stabilised rammed earth test building in the UK. Energy and Buildings 42 (6), 845–852.
URL http://dx.doi.org/10.1016/j.enbuild.2009.12.005

Almeida, G., Remond, R., Perré, P., 2010. Evidence of Dual-Scale Diffusion Mechanisms in Low Density Fibreboards : Experiment and Multiscale Modelling. Proceedings of the 17th International Drying Symposium (IDS'2010). pp. 1023–1030.

Almeida, G., Rémond, R., Perré, P., 2018. Hygroscopic behaviour of lignocellulosic materials: Dataset at oscillating relative humidity variations. Journal of Building Engineering 170, 716–724.

Challansonnex, A., Pierre, F., Casalinho, J., Lv, P., Perré, P., 2018. Mass diffusivity determination of various building materials based on inverse analysis of relative humidity evolution at the back face of a sample. Construction and Building Materials 193, 539 – 546.
URL http://www.sciencedirect.com/science/article/pii/S0950061818326369

Colinart, T., Lelievre, D., Glouannec, P., 2016. Experimental and numerical analysis of the transient hygrothermal behavior of multilayered hemp concrete wall. Energy and Buildings 112, 1–11.

Crank, J., 1953. A theoretical investigation of the influence of molecular relaxation and internal stress on diffusion in polymers. Journal of Polymer Science 11 (2), 151–168.

Crawley, D. B., Lawrie, L. K., Winkelmann, F. C., Buhl, W. F., Huang, Y. J., Pedersen, C. O., Strand, R. K., Liesen, R. J., Fisher, D. E., Witte, M. J., et al., 2001. Energyplus: creating a new-generation building energy simulation program. Energy and buildings 33, 319–331.

DeCarvalho, G., Frollini, E., DosSantos, W. N., 1996. Thermal conductivity of polymers by hot-wire method. Journal of Applied Polymer Science 62, 2281–2285.

Delgado, J., Ramos, N. M., Barreira, E., De Freitas, V., 2010. A critical review of hygrothermal models used in porous building materials. Journal of Porous Media 13, 221–234.

Feng, C., Janssen, H., Feng, Y., Meng, Q., 2015. Hygric properties of porous building materials: Analysis of measurement repeatability and reproducibility. Building and Environment 85, 160–172.

Hailwood, A., Horrobin, S., 1946. Absorption of water by polymers: analysis in terms of a simple model. Trans. Faraday Soc. 42B, 84–102.

Hens, H. L., 2015. Combined heat, air, moisture modelling: A look back, how, of help? Building and Environment 91, 138–151.

Hornung, U. (Ed.), 1997. Homogenization and porous media. Springer–Verlag, New York.

Lelievre, D., Colinart, T., Glouannec, P., 2014. Hygrothermal behavior of bio-based building materials including hysteresis effects: Experimental and numerical analyses. Energy and Buildings 84, 617–627.

Louërat, M., Ayouz, M., Perré, P., 2018. Heat and moisture diffusion in spruce and wood panels computed from 3-d morphologies using the lattice boltzmann method. International Journal of Thermal Sciences 130, 471–483.

Olek, W., Perré, P., Weres, J., 2011. Implementation of a relaxation equilibrium term in the convective boundary condition for a better representation of the transient bound water diffusion in wood. Wood science and technology 45, 677–691.

Olek, W., Romain, R., Weres, J., Perré, P., 2016. Non-fickian moisture diffusion in thermally modified beech wood analyzed by the inverse method. International Journal of Thermal Sciences 109, 291–298.

Osanyintola, O. F., Talukdar, P., Simonson, C. J., 2006. Effect of initial conditions, boundary conditions and thickness on the moisture buffering capacity of spruce plywood. Energy and Buildings 38, 1283–1292.

Perré, P., 2010. Multiscale modelling of drying as a powerful extension of the macroscopic approach: application to soid wood and biomass processing. Dry. Technol. 28 (8), 944–959.

Perré, P., 2015. The proper use of mass diffusion equations in drying modeling: Introducing the drying intensity number. Drying Technology 33, 1949–1962.

Perré, P., 2018. Coupled heat and mass transfer in lignocellulosic materials : a macroscopic formulation with non-Fickian effects suitable for Building Energy Simulation Tools. Submitted.

Perré, P., Pierre, F., Casalinho, J., Ayouz, M., 2015. Determination of the mass diffusion coefficient based on the relative humidity measured at the back face of the sample during unsteady regimes. Drying Technology 33, 1068–1075.

Perré, P., Remond, R., Turner, I. W., 2007. Comprehensive drying models based on volume averaging: Background, application and perspective. In: Tsotsas, E., Mujumdar, A. S. (Eds.), Drying Technology: Computational Tools at Different Scales. Vol. 1. Wiley-VCH.

Perré, P., Turner, I. W., 1999. A 3D version of Transpore: a comprehensive heat and mass transfer computational model for simulating the drying of porous media. International Journal for Heat and Mass Transfer 42, 4501–4521.

Rafidiarison, H., Rémond, R., Mougel, E., 2015. Dataset for validating 1-D heat and mass transfer models within building walls with hygroscopic materials. Building and Environment 89, 356–368.

Rémond, R., Almeida, G., 2011. Mass diffusivity of low-density fibreboard determined under steady- and unsteady-state conditions : Evidence of dual-scale mechanisms in the diffusion. Wood Material Science & Engineering 6, 23–33.

Rémond, R., Almeida, G., Perré, P., 2018. The gripped-box model: A simple and robust formulation of sorption hysteresis for lignocellulosic materials. Construction and Building Materials 170, 716–724.

Seng, B., Lorente, S., Magniont, C., 2017. Scale analysis of heat and moisture transfer through bio-based materials — Application to hemp concrete. Energy and Buildings 155, 546–558.

Steeman, M., Janssens, A., Steeman, H. J., Belleghem, M. V., Paepe, M. D., 2010. On coupling 1D non-isothermal heat and mass transfer in porous materials with a multizone building energy simulation model. Building and Environment 45, 865–877.

Vololonirina, O., Coutand, M., Perrin, B., 2014. Characterization of hygrothermal properties of wood-based products - Impact of moisture content and temperature. Construction and Building Materials 63, 223–233.

Wadsö, L., 1994. Describing non-Fickian water-vapour sorption in wood. Journal of Materials Science 29, 2367–2372.

Woloszyn, M., Rode, C., 2008. Tools for performance simulation of heat, air and moisture conditions of whole buildings. In: Building Simulation. Vol. 1. Springer, pp. 5–24.

Yi, S. Y., Fan, L. W., Fu, J. H., Xu, X., Yu, Z. T., 2016. Experimental determination of the water vapor diffusion coefficient of autoclaved aerated concrete (AAC) via a transient method: Effects of the porosity and temperature. International Journal of Heat and Mass Transfer 103, 607–610.

Zhang, M., Qin, M., Rode, C., Chen, Z., 2017. Moisture buffering phenomenon and its impact on building energy consumption. Applied Thermal Engineering 124, 337–345.